



Holographic near-eye display based on complex amplitude modulation with band-limited zone plates

YUN CHEN,^{1,2} MINJIE HUA,^{1,2} TIANSHUN ZHANG,^{1,2} MINGXIN ZHOU,^{1,2} JIANHONG WU,^{1,2,3} AND WENLONG ZOU^{1,2,4}

¹School of Optoelectronic Science and Engineering & Collaborative Innovation Center of Suzhou Nano Science and Technology, Soochow University, Suzhou 215006, China

²Key Lab of Advanced Optical Manufacturing Technologies of Jiangsu Province & Key Lab of Modern Optical Technologies of Education Ministry of China, Soochow University, Suzhou 215006, China

³jhwu@suda.edu.cn

⁴zouwenlong@suda.edu.cn

Abstract: A holographic near-eye display (NED) system based on complex amplitude modulation (CAM) with band-limited zone plates is proposed. The whole system mainly consists of a phase-only spatial light modulator (SLM), an Abbe-Porter filter system, an eyepiece, and an image combiner. The point source method based on band limited zone plates is used to accurately control the bandwidth of the target complex amplitude. The effects of intensity modulation coefficient γ in the frequency-filtering method on the intensity and the quality of reconstructed images are analyzed, which provide a judgment basis for selecting the appropriate value of γ . We also derive the expressions of the field of view (FOV) and exit pupil of the NED system. Since the holographic image is magnified in two steps in this system, the large FOV can be obtained. The optical experimental results show that the proposed system can provide a dynamic holographic three-dimensional (3D) augmented reality (AR) display with a 23.5° horizontal FOV.

© 2021 Optical Society of America under the terms of the [OSA Open Access Publishing Agreement](#)

1. Introduction

In recent years, with the development of computer science and display technology, augmented reality (AR) display has become a research hotspot in the next generation display technology. AR technology superimposes virtual images on the real environment [1], which expands the human visual perception ability. As carriers of AR technology, head up display (HUD) and near eye display (NED) have attracted more and more attention. Compared with the HUD, the NED device has the characteristics of compactness and wearability, which provides an excellent visual immersion experience for the observer. However, most NED devices provide the observer with a three-dimensional (3D) effect based on binocular parallax, which leads to the accommodation-convergence conflict (A-V) [2] that may make the observer feel dizzy and visual fatigue.

To overcome the A-V conflict, there have been many works applying relevant 3D display technology to NED devices, such as Integral imaging [3–5], Super multi-view display [6–8], Maxwellian display [9–11], Holographic display [12–18], etc. Compared with other 3D display technologies, holographic display can reconstruct 3D images with real physical depth because it records the wavefront information of the object, which is an ideal true 3D display technology. Yeom et al. designed a bar-type 3D holographic NED [12], which consists of two holographic optical elements (HOE) as input and output couplers, and the astigmatism of this system is corrected by the wavefront modulation of the spatial light modulator (SLM). Chen et al. proposed a solution for a large viewing angle holographic NED system [13]. It uses divergent light to illuminate the hologram to reconstruct a large-scale 3D object within a short distance and achieve

a viewing angle of more than 60° . Xia et al. designed a holographic NED system with a HOE [14]. The HOE is fabricated by the interference between the object light which passed through the micro-lens array and the reference light, and it is used as an image combiner to achieve a 10 mm eyebox. In order to obtain higher diffraction efficiency, a phase-only SLM is used to load Kinoform in these holographic NED systems mentioned above, which requires an iterative algorithm to compensate for the loss of amplitude. Due to the introduction of random phase, serious speckle noises have appeared in the reconstructed image.

Compared with the iterative algorithm, the complex amplitude modulation (CAM) algorithm [19–25] completely preserves the amplitude and phase information to make the reconstructed images have a high quality. The CAM algorithms currently used in holographic NED are mainly double-phase method [22] and frequency-filtering method [25]. Compared with the double-phase method that often uses a grating to achieve beam combination, the latter has higher diffraction efficiency and relatively simple optical system. However, due to the limited space bandwidth product (SBP) of the SLM, when the bandwidth of the target complex amplitude is too large, crosstalk is likely to occur between orders of the frequency spectrum of the hologram, so how to accurately control the bandwidth of the complex amplitude is a problem worthy of consideration. In addition, the previous research on the frequency-filtering method have not analyzed how the intensity modulation coefficient γ (which is the coefficient β in [20]) affects the intensity and the quality of the reconstructed image. The specific analysis of this problem will help us choose the appropriate value of γ , to achieve a balance between the intensity and quality of the reconstructed image. In holographic display, the main methods to obtain the complex amplitude distribution of the target object on the hologram are point source method [26], polygon-based method [27] and layer-based method [28]. Among these methods, the point source method is more flexible and can reconstruct objects with complex structures. To make the NED system more compact, these point sources need to be close to the hologram. When the recording distance of the point source is short, in order to avoid under-sampling of the hologram, the maximum spatial frequency can be $1/2p$ (p is the pixel pitch of the SLM) by reducing the size of the zone plate [29]. This means that we can accurately control the bandwidth of the target complex amplitude by changing the size of zone plates in a compact NED system.

In this paper, a holographic NED system based on CAM with band-limited zone plates is proposed. The frequency-filtering method is used to reconstruct target images. To accurately control the bandwidth of the target complex amplitude and realize reconstruction for short distance, the point source method based on band-limited zone plates is used to calculate the complex amplitude distribution of the target object. We also analyze the effects of the intensity modulation coefficient γ on the intensity and the quality of the reconstructed image in detail. Then the holographic NED system is analyzed, and the expressions of the FOV and exit pupil of the system are given. Finally, the optical experimental results show that the holographic NED system can provide high quality images and dynamic AR displays with large FOV.

2. System and principle

2.1. Proposed holographic NED system

The proposed holographic NED system is shown in Fig. 1. It is mainly composed of a phase-only SLM, an Abbe-Porter filter system, an eyepiece, and an image combiner. To make the frequency spectrum of the target complex amplitude at the center of the Fourier domain, a collimated oblique beam is used to illuminate the SLM. Then the modulated light passes through the Abbe-Porter filter system composed of Lens1 and a band-pass filter. In this process, since only the frequency spectrum of the target complex amplitude passes the filter, the holographic image is magnified. The magnified holographic image is called intermediate image. Compared with the 4f filter system, the used filter system reduces the number of optical components. According to the Gaussian imaging principle, when the magnification is determined, the Lens1 with a short

focal length can shorten its object distance and image distance, so that the system will be more compact, however, the holographic recording distance also needs to be shortened at this time. The intermediate image is located within the focal length of Lens2 that is an eyepiece to form a magnified virtual image. A beam splitter (BS) as an image combiner is placed behind the Lens2 to turn the light path, and the magnified virtual image and the external environment can be simultaneously observed through the combiner. The holographic image is magnified in two steps in this system, so the AR display with large FOV can be obtained. The proposed holographic NED system is analyzed in detail in section 2.5.

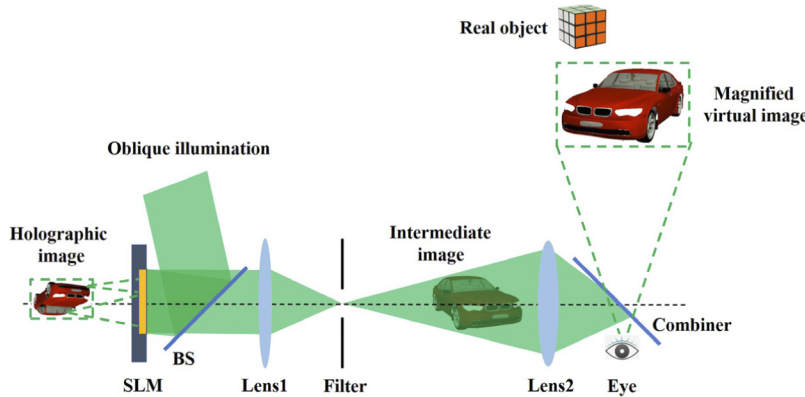


Fig. 1. Schematic diagram of holographic NED system.

2.2. Principle of complex amplitude modulation algorithm

The complex amplitude distribution of the target object on the hologram is:

$$U(x, y) = A(x, y)\exp[j\varphi_o(x, y)] \quad (1)$$

Where $A(x, y)$ is the normalized amplitude distribution of the target wavefront, $\varphi_o(x, y)$ is the phase distribution of the target wavefront, and j is the imaginary unit. By introducing the reference light to transform the amplitude and phase into a phase-only hologram function, which can be expressed as:

$$H(x, y) = \exp\{j\gamma A(x, y) \cos[\varphi_o(x, y) - \varphi_r(x, y)]\} \quad (2)$$

Where γ is the intensity modulation coefficient, $\varphi_r(x, y)$ is the phase distribution of the reference light. The phase-only hologram function is transformed into the following expression by using Bessel's identity [30]:

$$H(x, y) = \sum_{n=-\infty}^{\infty} J_n[\gamma A(x, y)] j^n \exp\{-jn[\varphi_o(x, y) - \varphi_r(x, y)]\} \quad (3)$$

Where $J_n(*)$ is the n -th order of the Bessel function of the first kind. Because $J_{-1}(*) = -J_1(*)$, the target amplitude and phase are included in the -1 order of Eq. (3). When $\gamma A(x, y)$ is small, according to the series expansion of the Bessel function, the -1 order can be approximately expressed as:

$$H_{(-1)}(x, y) \approx j\gamma A(x, y) \exp\{j[\varphi_o(x, y) - \varphi_r(x, y)]\} \quad (4)$$

When the appropriate carrier frequency of reference light is selected, the frequency spectrum of each order can be separated in the Fourier domain after Fourier transform of the hologram

function, and then the frequency spectrum of the required -1 order can be filtered to reconstruct the target complex amplitude, so this CAM algorithm is called frequency-filtering method. To make the frequency spectrum of the -1 order at the center of the Fourier domain, an oblique beam conjugated with the reference light can be used for illumination. The expression of the -1 order is:

$$H'_{(-1)}(x, y) \approx j\gamma A(x, y)\exp[j\varphi_o(x, y)] \quad (5)$$

2.3. Point source method based on band-limited zone plates

The bandwidth of the target complex amplitude is further limited because the carrier frequency is introduced in frequency-filtering method. The maximum bandwidth of the target complex amplitude can only be $1/2p$ without considering that the zero order has a certain bandwidth. If the bandwidth can be accurately controlled, under-sampling can be avoided in short-distance recording and an appropriate carrier frequency can be selected to separate all orders on the frequency spectrum of the hologram. The relationship between the carrier frequency and the bandwidth is given in section 2.4. As shown in Fig. 2(a), the target object can be regarded as composed of a series of self-illuminated point sources. Each point source corresponds to a zone plate on the hologram, but each zone plate does not occupy the entire hologram. The complex amplitude distribution of the zone plate is:

$$u_i(x_i, y_i) = \frac{a_i}{r_i} \exp(jkr_i) \quad (6)$$

Where x_i and y_i are the coordinates of the contribution area of each zone plate on the hologram, a_i is the amplitude information of the i -th point source, $r_i = \sqrt{x_i^2 + y_i^2 + z_i^2}$ is the distance from the i -th point source to any point on its zone plate, z_i is the distance from the point source to the hologram, and k is the wave number. When zone plates corresponding to all point sources are superimposed on the hologram, the complex amplitude distribution of the target object can be expressed as:

$$U(x, y) = \sum_{i=1}^S u_i(x_i, y_i) \quad (7)$$

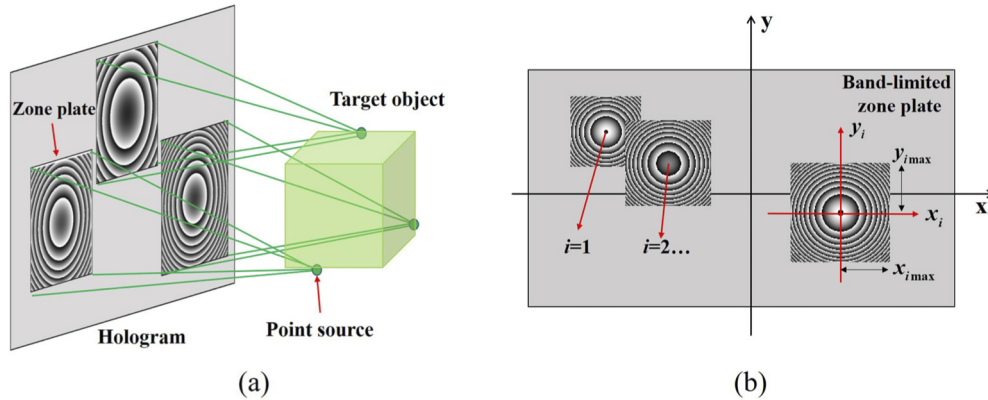


Fig. 2. (a) Each point source of the target object corresponds to a zone plate on the hologram.
(b) The hologram is calculated based on band-limited zone plates.

Where x and y are the coordinates on the entire hologram, S is the total number of point sources.

As shown in Fig. 2(b), the maximum spatial frequency in the x_i and y_i direction of each zone plate can be expressed as:

$$\begin{aligned} f_{x_{i \max}} &= x_{i \max} / (\lambda z_i) \\ f_{y_{i \max}} &= y_{i \max} / (\lambda z_i) \end{aligned} \quad (8)$$

Where $x_{i \max}$ and $y_{i \max}$ are the maximum boundary positions starting from the center of the zone plate, and λ is the illumination wavelength. Equation (8) also shows that when the bandwidth of the target complex amplitude that meets the filtering requirement is determined, the size of the zone plate corresponding to each point source on the hologram can be calculated as:

$$\begin{aligned} M_i &\approx 2F_{x \max} \lambda z_i / p \\ N_i &\approx 2F_{y \max} \lambda z_i / p \end{aligned} \quad (9)$$

Where M_i and N_i represent the size of the zone plate in the x_i and y_i directions, $F_{x \max}$ and $F_{y \max}$ are the maximum spatial frequency of the target complex amplitude in the x and y directions without considering the carrier frequency, and p is the sampling interval on the hologram. In other words, the bandwidth of the target complex amplitude can be controlled by changing the size of zone plates, so it is called band-limited zone plates in this paper.

To illustrate that the use of band-limited zone plates in the frequency-filtering method can accurately control the bandwidth of the target complex amplitude, Fig. 3 shows the simulation results of using ‘Cameraman’ and ‘Mandrill’ as target images under different bandwidths. These two target images are 768×768 grayscale images, the hologram resolution is 1920×1080 , $p = 8 \mu\text{m}$, $\gamma = 1$ and the reconstructed distance is 50 mm. The bandwidth of the target complex amplitude is set as $1/2p$, $1/3p$ and $1/4p$ respectively, so the corresponding $F_{x \max}$ is $1/4p$, $1/6p$ and $1/8p$ (the same bandwidth in both directions). Therefore, according to Eq. (9), the size of zone plates corresponding to each bandwidth can be calculated as 207×207 , 137×137 , 103×103 respectively. The local enlarged parts of two reconstructed images are marked with red solid lines to more clearly show the change in resolution in Fig. 3. As can be seen from Figs. 3(a)–(f), the resolution of the image decreases with the reduction of the size of the zone plate. This shows that the band-limited zone plate is an effective and flexible method to control the bandwidth of the target complex amplitude. It can also be seen that on the basis of accurately controlling the bandwidth, the frequency-filtering method is used to make the reconstructed image have a higher quality and no speckle noises.

2.4. Effects of Intensity modulation coefficient γ on the reconstructed image

Here, the effects of the intensity modulation coefficient γ on the intensity and the quality of the reconstructed image are analyzed specifically. Since frequency-filtering is a key step to reconstruct the target image, the effect of γ on the intensity of each order of the frequency spectrum is analyzed here to equivalent illustrate its effect on the intensity of the reconstructed image. According to Eq. (3), the intensity of each order of the frequency spectrum can be expressed as:

$$I_n = \sum_{p=1}^P \sum_{q=1}^Q |\mathcal{F}\{H_{(n)}\}|^2 \quad (10)$$

Where $P \times Q$ is the number of sampling points of each order of intensity distribution, $\mathcal{F}(*)$ represents the Fourier transform, and n is the ordinal number of each order. First, we conduct a numerical simulation to illustrate the effect of γ on the intensity of each order of the frequency spectrum. The three grayscale images ‘Cameraman’, ‘Mandrill’ and ‘Liftingbody’ are used as target images and are marked as ‘target image_1’, ‘target image_2’ and ‘target image_3’ in Fig. 4. The size of these target images is 768×768 , the reconstructed distance is 50 mm, the zone plate size is 207×207 , the hologram resolution is 1920×1080 , and p is $8 \mu\text{m}$. Figure 4(a) shows that the

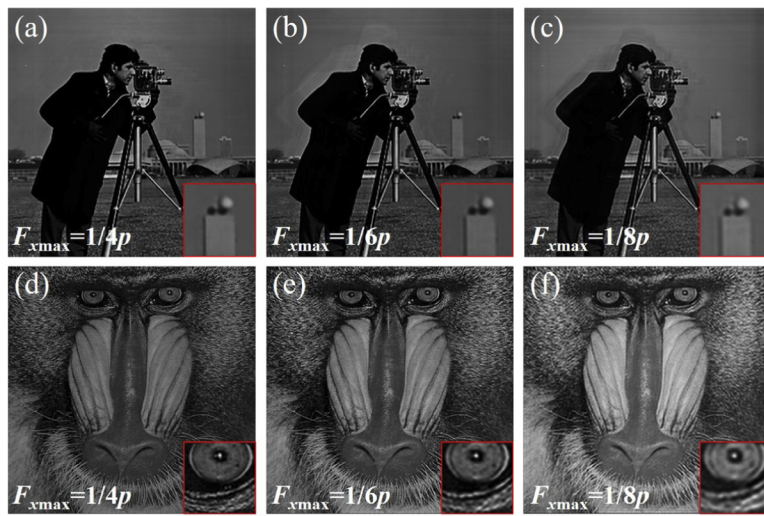


Fig. 3. Simulation results of band-limited zone plates control the bandwidth. (a)-(c) are the simulated reconstruction results of ‘Cameraman’ under different bandwidths. (d)-(f) are the simulated reconstruction results of ‘Mandril’ under different bandwidths.

relationship between the relative intensity of each order of the frequency spectrum and intensity modulation coefficient. The relative intensity here refers to the intensity of each order relative to the zero order after all simulation data are normalized. In Fig. 4(a), different colors are used to represent different orders and different types of lines are used to represent curves corresponding to different target images. Since the various orders are symmetrically distributed about the zero order, only the intensity curves corresponding to the 0, -1, -2 and -3 order are shown in Fig. 4(a). The simulation results show that the change trends of curves corresponding to different target images are consistent. Specifically, the intensity of zero order decreases with the increase of γ , while the intensity of other orders increases firstly and then decreases. This change indicates that the energy is transferred from zero order to other orders by changing γ , so that the intensity of -1 order can be improved by selecting the appropriate value of γ , and the intensity of the corresponding reconstructed image has also been improved.

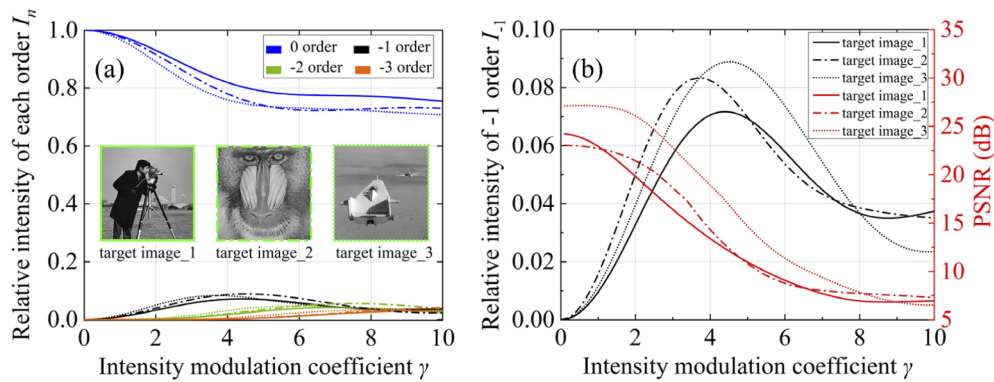


Fig. 4. (a) The relationship between the relative intensity of each order of the frequency spectrum and the intensity modulation coefficient γ with different target images. (b) The relationship between the intensity of -1 order of the frequency spectrum and the PSNR of the reconstructed image with different target images.

Then we also find that the quality of the reconstructed image changes as the γ changes. The peak signal-to-noise ratio (PSNR) is introduced to evaluate the quality of the reconstructed image. In order to show the relationship between the intensity and the PSNR of the reconstructed image, three black curves in Fig. 4(a) with different types representing the intensity of -1 order of the frequency spectrum corresponding to different target images and the three corresponding PSNR curves are all drawn in Fig. 4(b). For different target images, the change trend of the intensity and the PSNR with the change of γ are consistent as shown in Fig. 4(b). There is a trade-off between the intensity of the -1 order and the quality of the reconstructed image before the intensity of the -1 order reaches the maximum in Fig. 4(b). But with the increase of γ , the PSNR of the reconstructed image is always decreasing. Because the $\gamma A(x, y)$ in Eq. (4) is no longer a small amount, so the error between the amplitude distribution of the -1 order of the hologram and the amplitude distribution of the target complex amplitude becomes larger. Therefore, the value of γ should be selected in the range that satisfies the above trade-off relationship. For example, for the target imgae_1, $I_{-1}=0.002$, PSNR=23.89 dB ($\gamma=0.5$); $I_{-1}=0.038$, PSNR=19.12 dB ($\gamma=2.2$); $I_{-1}=0.067$, PSNR=14.53 dB ($\gamma=3.6$). Where $\gamma=2.2$, a higher intensity and higher quality reconstructed image can be obtained. The analysis of the intensity and the PSNR in Fig. 4(b) provides a judgment basis for selecting the appropriate value of γ , so that the balance between the intensity and quality of the reconstructed image can be achieved.

Furthermore, it can be seen from Fig. 4(a) that even if the intensity of the -1 order reaches the maximum, the intensity of high orders is still very low, and due to the SBP of the SLM is limited, the information of high orders cannot be expressed, so the effect of these orders on the reconstructed image can be ignored. Therefore, it is only necessary to consider whether the 0 and -1 order are separated when filtering. Since the cutoff frequency f_c on the spectrum is $1/2p$, it means that the maximum bandwidth of the -1 order is $1/2p$ without considering the bandwidth of the zero order. If the bandwidth of the -1 order is too large, the information beyond the cutoff frequency will not be expressed, and in severe cases, it will lead to under-sampling of the hologram. Choosing a suitable carrier frequency of reference light can avoid crosstalk of each order. When f_r is the carrier frequency along the x direction, f_0 is the half of the bandwidth of the zero order, and f_{-1} is the half of the bandwidth of the -1 order, then the relationship that the carrier frequency needs to satisfy is $f_0+f_{-1} \leq f_r \leq f_c-f_{-1}$.

2.5. Analysis of holographic NED system

In order to facilitate the analysis of the FOV and the size of the exit pupil of the proposed NED system, the optical system is simplified as the equivalent optical path shown in Fig. 5. The optical path is actually the microscope system, including an objective lens (Lens1), an eyepiece (Lens2), and a band-pass filter. The sign rule followed when analyzing the optical path is: starting from the principal plane of the lens, the line segment is positive from left to right, and negative from right to left. The focal length of the Lens1 is f_1' , the corresponding object distance and image distance are l_1 and l_1' respectively, and the magnification is β_1 . The relationship between these four quantities is:

$$l_1' = (1 - \beta_1)f_1' \quad (11)$$

For meeting the requirements of a compact system, l_1' needs to be shortened. In the case of a certain magnification, the shorter the focal length, the shorter the image distance and the object distance. Then the intermediate image located within the focal length of the Lens2 is magnified as a virtual image, the object distance is l_2 , the image distance is l_2' , and the focal length is f_2' , then the magnification can be expressed as:

$$\beta_2 = 1/(1 + l_2/f_2') \quad (12)$$

It can be seen from the above equation that when the object is within one focal length, the shorter the focal length, the higher the magnification. If the Lens 2 is replaced by a reflective

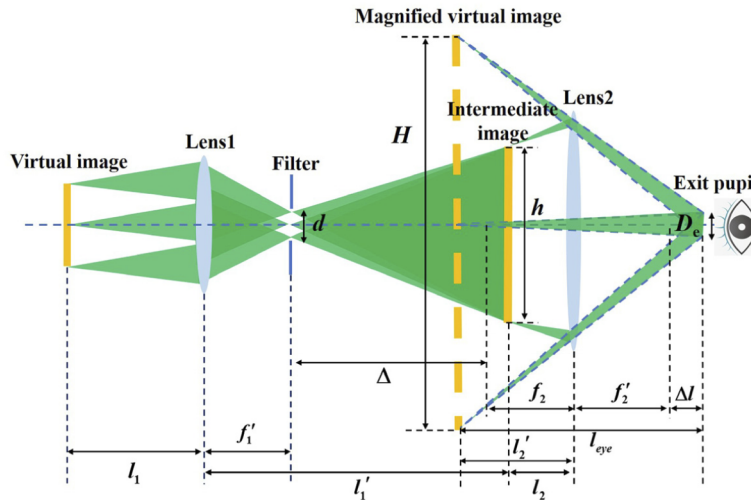


Fig. 5. Schematic diagram of optical path of holographic NED system.

HOE, it can achieve augmented reality while imaging and make the system more compact. The band-pass filter is equivalent to the aperture stop at the front focus of the Lens1, so the exit pupil of the system is at the back focus of the entire system. The distance between the exit pupil and the back focus of Lens2 is Δl , and its expression is:

$$\Delta l = f'_2^2 / \Delta \quad (13)$$

Where Δ is the distance between the back focus of the Lens1 and the front focus of the Lens2. The human eye can observe the complete image at the exit pupil. The FOV of the NED system is positively correlated with the image size, and here we define the FOV as:

$$FOV = 2 \tan^{-1}(H/2l_{eye}) \quad (14)$$

Where H is the width of the virtual image, and the observation distance is $l_{eye} = f'_2 - l'_2 + \Delta l$. For the entire system, the exit pupil is the real image of -1 order of the frequency spectrum formed by Lens2, so the size of the exit pupil can be expressed as:

$$D_e = f'_2 d / \Delta \quad (15)$$

Where the aperture of the filter is $d = 2F_{\text{max}}\lambda f'_1$. From the above equation, when other quantities remain unchanged, a larger exit pupil can be obtained by using an SLM with a larger SBP.

3. Experiment and results

We built an optical setup as shown in Fig. 6 to demonstrate the proposed holographic NED system. The incident wavelength of the laser is 532 nm, the used phase-only SLM (Holoeye Pluto VIS-016) with 1920×1080 pixels, 8 μm pixel pitch, 60 fps refresh rate, and the phase modulation range is [0, 2π]. And the focal length of Lens1 and Lens2 are 125 mm and 50 mm respectively. The image combiner is a beam splitter. A camera (Canon EOS 6D Mark II) was used to simulate the human eye to capture reconstructed images.

Firstly, the experimental results of the effects of the intensity modulation coefficient γ on the intensity and the quality of the reconstructed image are given, as shown in Fig. 7. A 768×768

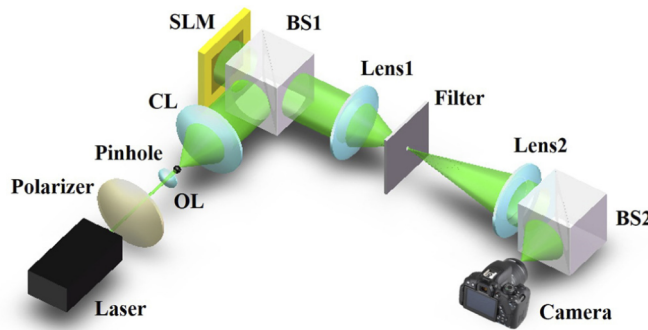


Fig. 6. Schematic illustration of the experimental system for the proposed holographic NED.

grayscale image ‘Cameraman’ is selected as the target image. In the experiment, considering that the zero order of the frequency spectrum has a certain bandwidth, in order to reduce the interference to the reconstructed image, the half of the bandwidth of the target complex amplitude is set to 28 lp/mm, and the carrier frequency of the reference light (x direction) is 31.25 lp/mm. When the recording distance is 67.5 mm, the size of the band-limited zone plate is about 251×251. Figures 7(a)–(d) and (e)–(h) respectively show the numerical simulation and optical experiment results under $\gamma=0.5$, $\gamma=2.5$, $\gamma=3.5$, and $\gamma=5$. With the increase of γ , the intensity and quality of the reconstructed image are changing, and the simulation and experimental results are consistent. Figure 7(e) has the best quality but the lowest intensity, Fig. 7(h) has the worst quality. Among these reconstructed images, Fig. 7(f) achieves a balance between intensity and quality, so $\gamma=2.5$ is the appropriate intensity modulation coefficient we should choose. The above results show that with the increase of γ , the quality of the image becomes worse and worse as the intensity changes, which is consistent with the conclusion analyzed in section 2.4.

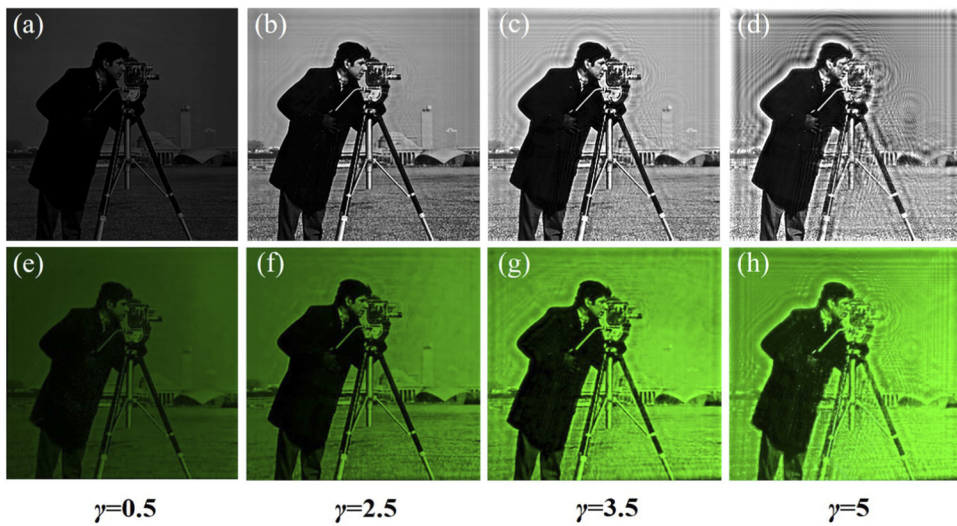


Fig. 7. Experimental results of the effects of intensity modulation coefficient γ on the reconstructed image. (a)–(c) are the numerical simulation results respectively. (d)–(e) are the optical reconstruction results.

Then the depth information expression of the reconstructed image was tested through optical experiments. The school badge pattern and the character ‘SOOCHOW UNIVERSITY’ are selected as the target images. The half of the bandwidth of the target complex amplitude is set to 28 lp/mm, the carrier frequency (x direction) is 31.25 lp/mm, and $\gamma=2$. Two target images are reconstructed 130 mm and 1000 mm away from the camera respectively, and two real objects (a doll and a toy car) were placed at the same depth with two target images. The size of the exit pupil is about 0.81 mm and a horizontal FOV of about 17.8° can be obtained. In Figs. 8(a)–(b), the yellow and red dashed lines mark the partial enlarged images of the two reconstructed images. As shown in Fig. 8(a), when the camera is focused on the school badge, the school badge is clear, while the character ‘SOOCHOW UNIVERSITY’ is blurred. As shown in Fig. 8(b), when the camera focuses on the character ‘SOOCHOW UNIVERSITY’, the character is clear, while the school badge is blurred. Experimental results show that the system can provide a 3D reconstructed image with correct depth information and can achieve an AR display with a larger FOV.

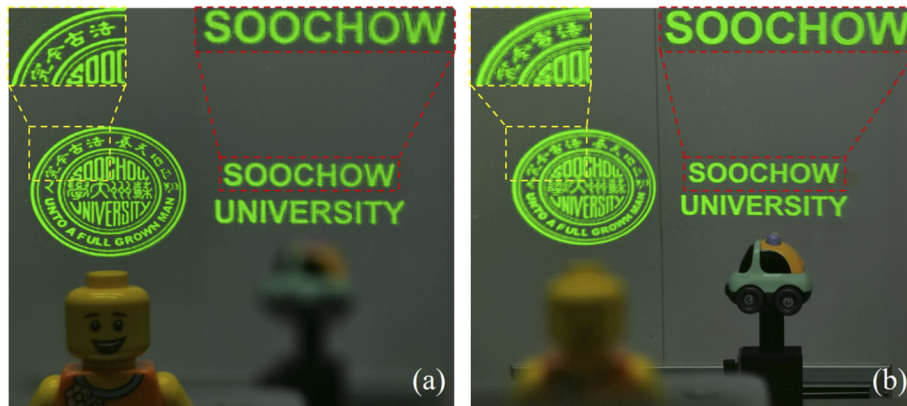


Fig. 8. The depth information expression of the reconstructed image. (a) The school badge is focused at 130 m from the camera. (b) The character is focused at 1000 m from the camera.

Finally, the system’s ability to provide dynamic holographic 3D augmented reality displays was tested. The dynamic 3D model used in the experiment is a 360° horizontally rotating car, and the dynamic video refresh rate is 24fps. The half of the bandwidth of the target complex amplitude is 28 lp/mm, the carrier frequency (x direction) is 31.25 lp/mm, and $\gamma=2.5$. The target model is reconstructed 400 mm away from the camera, the size of the exit pupil is about 0.76 mm, and the measurement shows that the horizontal FOV is about 23.5° . The video is recorded in [Visualization 1](#). Figures 9(a)–(f) shows six frames of images of the dynamically rotating car, from which the reconstructed images have high quality. The experimental results prove that the holographic NED system proposed in this paper can provide dynamic holographic 3D augmented reality display.

It should be noted that to obtain a larger FOV in the above experiments, the size of the exit pupil is very small, which leads to a larger depth of field (DOF) of the system and weakens the depth perception. According to Eq. (15), the size of the exit pupil is proportional to the bandwidth of the target complex amplitude. Therefore, we can adopt a SLM with smaller pixel pitch to obtain a larger size of the exit pupil in future research, so as to better show the depth change.

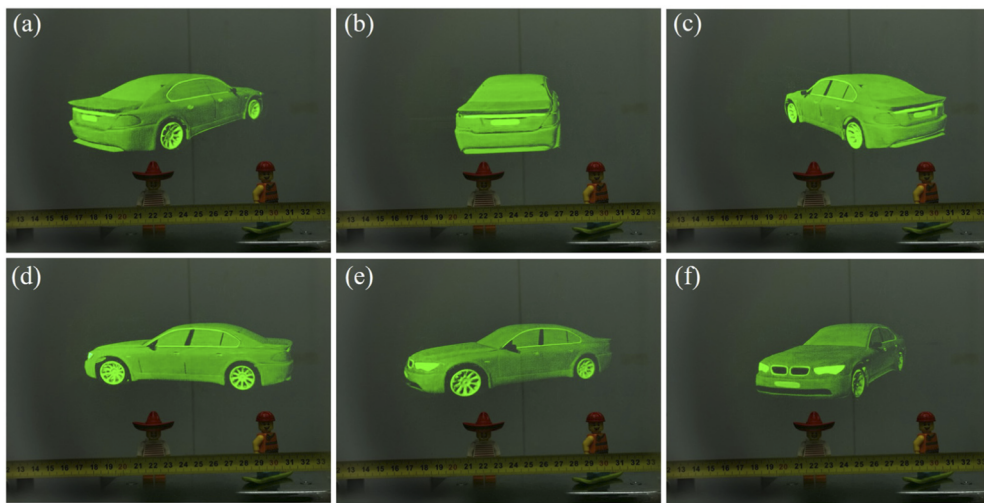


Fig. 9. Dynamic holographic 3D AR display (Visualization 1). (a)-(f) are the six extracted frames from the video.

4. Conclusion

We have proposed a holographic NED system based on CAM with band-limited zone plates. The frequency-filtering method is used to reconstruct target images. The holographic image is magnified in two steps by an Abbe-Porter filter system and an eyepiece, so the AR display with large FOV can be obtained. The point source method based on band-limited band plates is used to accurately control the bandwidth of the target complex amplitude. The effects of intensity modulation coefficient γ on the intensity and the quality of the reconstructed image are also analyzed, which provide a judgment basis for the selection of an appropriate value of γ . The expressions of the FOV and exit pupil of the system are derived. The larger FOV and exit pupil can be obtained by using a SLM with larger SBP in the future. The optical experiment result shows that the system can provide a 3D reconstructed image with correct depth information, and can achieve a dynamic holographic 3D AR display with a horizontal 23.5° FOV.

Funding. Priority Academic Program Development of Jiangsu Higher Education Institutions.

Disclosures. The authors declare no conflicts of interest.

Data availability. Data underlying the results presented in this paper are not publicly available at this time but may be obtained from the authors upon reasonable request.

References

1. J. Carmignani, B. Furht, M. Anisetti, P. Ceravolo, E. Damiani, and M. Ivkovic, "Augmented reality technologies, systems and applications," *Multimed Tools Appl* **51**(1), 341–377 (2011).
2. Jason and Geng, "Three-dimensional display technologies," *Adv. Opt. Photon.* **5**(4), 456–535 (2013).
3. H. Huang and H. Hua, "High-performance integral-imaging-based light field augmented reality display using freeform optics," *Opt. Express* **26**(13), 17578–17590 (2018).
4. H. Hua and B. Javidi, "A 3D integral imaging optical see-through head-mounted display," *Opt. Express* **22**(11), 13484–13491 (2014).
5. X. Shen and B. Javidi, "Large depth of focus dynamic micro integral imaging for optical see-through augmented reality display using a focus-tunable lens," *Appl. Opt.* **57**(7), B184–B189 (2018).
6. Y. Takaki, K. Tanaka, and J. Nakamura, "Super multi-view display with a lower resolution flat-panel display," *Opt. Express* **19**(5), 4129–4139 (2011).
7. T. Ueno and Y. Takaki, "Super multi-view near-eye display to solve vergence-accommodation conflict," *Opt. Express* **26**(23), 30703–30715 (2018).
8. T. Ueno and Y. Takaki, "Approximated super multi-view head-mounted display to reduce visual fatigue," *Opt. Express* **28**(9), 14134–14150 (2020).

9. S.-B. Kim and J.-H. Park, "Optical see-through Maxwellian near-to-eye display with an enlarged eyebox," *Opt. Lett.* **43**(4), 767–770 (2018).
10. P. K. Shrestha, M. J. Pryn, J. Jia, J.-S. Chen, H. N. Fructuoso, A. Boev, Q. Zhang, and D. Chu, "Accommodation-Free Head Mounted Display with Comfortable 3D Perception and an Enlarged Eye-box," *Research* (Washington, D.C.) 20199273723–9273723 (2019).
11. T. Lin, T. Zhan, J. Zou, F. Fan, and S.-T. Wu, "Maxwellian near-eye display with an expanded eyebox," *Opt. Express* **28**(26), 38616–38625 (2020).
12. H.-J. Yeom, H.-J. Kim, S.-B. Kim, H. Zhang, B. Li, Y.-M. Ji, S.-H. Kim, and J.-H. Park, "3D holographic head mounted display using holographic optical elements with astigmatism aberration compensation," *Opt. Express* **23**(25), 32025–32034 (2015).
13. Z. Chen, X. Sang, Q. Lin, J. Li, X. Yu, X. Gao, B. Yan, K. Wang, C. Yu, and S. Xie, "A see-through holographic head-mounted display with the large viewing angle," *Optics Communications* **384**, 125–129 (2017).
14. X. Xia, Y. Guan, A. State, P. Chakravarthy, and H. Fuchs, "Towards Eyeglass-style Holographic Near-eye Displays with Statically Expanded Eyebox," in *2020 IEEE International Symposium on Mixed and Augmented Reality (ISMAR)* (2020).
15. W.-K. Lin, O. Matoba, B.-S. Lin, and W.-C. Su, "Astigmatism and deformation correction for a holographic head-mounted display with a wedge-shaped holographic waveguide," *Appl. Opt.* **57**(25), 7094–7101 (2018).
16. C. Chang, W. Cui, and L. Gao, "Holographic multiplane near-eye display based on amplitude-only wavefront modulation," *Opt. Express* **27**(21), 30960–30970 (2019).
17. A. Maimone, A. Georgiou, and J. S. Kollin, "Holographic Near-Eye Displays for Virtual and Augmented Reality," *ACM Trans. Graph.* **36**(4), 1–16 (2017).
18. M. Choi, Y.-G. Ju, and J.-H. Park, "Holographic near-eye display with continuous expanded eyebox using two-dimensional replication and angular spectrum wrapping," *Opt. Express* **28**(1), 533–547 (2020).
19. O. Mendoza-Yero, G. Minguez-Vega, and J. Lancis, "Encoding complex fields by using a phase-only optical element," *Opt. Lett.* **39**(7), 1740–1743 (2014).
20. X. Li, J. Liu, J. Jia, Y. Pan, and Y. Wang, "3D dynamic holographic display by modulating complex amplitude experimentally," *Opt. Express* **21**(18), 20577–20587 (2013).
21. Q. Gao, J. Liu, J. Han, and X. Li, "Monocular 3D see-through head-mounted display via complex amplitude modulation," *Opt. Express* **24**(15), 17372–17383 (2016).
22. Q. Gao, J. Liu, X. Duan, T. Zhao, X. Li, and P. Liu, "Compact see-through 3D head-mounted display based on wavefront modulation with holographic grating filter," *Opt. Express* **25**(7), 8412–8424 (2017).
23. Z. Zhang, J. Liu, X. Duan, and Y. Wang, "Enlarging field of view by a two-step method in a near-eye 3D holographic display," *Opt. Express* **28**(22), 32709–32720 (2020).
24. S. Choi, J. Kim, Y. Peng, and G. Wetzstein, "Optimizing image quality for holographic near-eye displays with Michelson Holography," *Optica* **8**(2), 143–146 (2021).
25. W. Song, X. Li, Y. Zheng, Y. Liu, and Y. Wang, "Full-color retinal-projection near-eye display using a multiplexing-encoding holographic method," *Opt. Express* **29**(6), 8098–8107 (2021).
26. H. Zhang, N. Collings, J. Chen, B. Crossland, D. Chu, and J. Xie, "Full parallax three-dimensional display with occlusion effect using computer generated hologram," *Opt. Eng.* **50**(7), 074003 (2011).
27. W. Lee, D. Im, J. Paek, J. Hahn, and H. Kim, "Semi-analytic texturing algorithm for polygon computer-generated holograms," *Opt. Express* **22**(25), 31180–31191 (2014).
28. Y. Zhao, L. Cao, H. Zhang, D. Kong, and G. Jin, "Accurate calculation of computer-generated holograms using angular-spectrum layer-oriented method," *Opt. Express* **23**(20), 25440–25449 (2015).
29. T. Shimobaba, N. Masuda, and T. Ito, "Simple and fast calculation algorithm for computer-generated hologram with wavefront recording plane," *Opt. Lett.* **34**(20), 3133–3135 (2009).
30. J. W. Goodman, *Introduction to Fourier Optics* (Roberts & Company Publishers, 2005).